Covalent 2D Cr$_2$Te$_3$ ferromagnet

Mengying Bian , Aleksandr N. Kamenskii , Mengjiao Han , Wenjie Li , Sichen Wei , Xuezeng Tian , David B. Eason , Fan Sun , Keke He , Haolei Hui , Fei Yao , Renat Sabirianov , Jonathan P. Bird , Chunlei Yang , Jianwei Miao , Junhao Lin , Scott A. Crooker , Yanglong Hou & Hao Zeng

MATERIALS RESEARCH LETTERS

Taylor & Francis
Taylor & Francis Group

ORIGINAL REPORT

🔓 OPEN ACCESS   Check for updates

Covalent 2D Cr2Te3 ferromagnet

Mengying Bian[a,b], Aleksandr N. Kamenskii[c,d], Mengjiao Han[e], Wenjie Li[f], Sichen Wei[g], Xuezeng Tian[h], David B. Eason[g], Fan Sun[b], Keke He[i], Haolei Hui[b], Fei Yao[g], Renat Sabirianov[j], Jonathan P. Bird[i], Chunlei Yang[f], Jianwei Miao[h], Junhao Lin[e], Scott A. Crooker[c], Yanglong Hou[a] and Hao Zeng[b]

[a]Beijing Key Laboratory for Magnetoelectric Materials and Devices and Beijing Innovation Center for Engineering Science and Advanced Technology, Department of Materials Science and Engineering, Peking University, Beijing, People's Republic of China; [b]Department of Physics, University at Buffalo, The State University of New York, Buffalo, NY, USA; [c]National High Magnetic Field Laboratory, Los Alamos National Laboratory, Los Alamos, NM, USA; [d]Experimentelle Physik II, Technische Universität Dortmund, Dortmund, Germany; [e]Department of Physics and Shenzhen Key Laboratory for Advanced Quantum Functional Materials and Devices, Southern University of Science and Technology, Shenzhen, People's Republic of China; [f]Center for Information Photonics and Energy Materials, Shenzhen Institutes of Advanced Technology, Chinese Academy of Sciences, People's Republic of China; [g]Department of Materials Design and Innovation, University at Buffalo, The State University of New York, Buffalo, NY, USA; [h]Department of Physics & Astronomy and California NanoSystems Institute, University of California, Los Angeles, CA, USA; [i]Department of Electrical Engineering, University at Buffalo, The State University of New York, Buffalo, NY, USA; [j]Department of Physics, University of Nebraska-Omaha, Omaha, NE, USA

ABSTRACT
To broaden the scope of van der Waals 2D magnets, we report the synthesis and magnetism of covalent 2D magnetic Cr_2Te_3 with a thickness down to one-unit-cell. The 2D Cr_2Te_3 crystals exhibit robust ferromagnetism with a Curie temperature of 180 K, a large perpendicular anisotropy of $7 \times 10^5\,J\,m^{-3}$, and a high coercivity of ~ 4.6 kG at 20 K. First principles calculations further show a transition from canted to collinear ferromagnetism, a transition from perpendicular to in-plane anisotropy, and emergent half-metallic behavior in atomically-thin Cr_2Te_3, suggesting its potential application for injecting carriers with high spin polarization into spintronic devices.
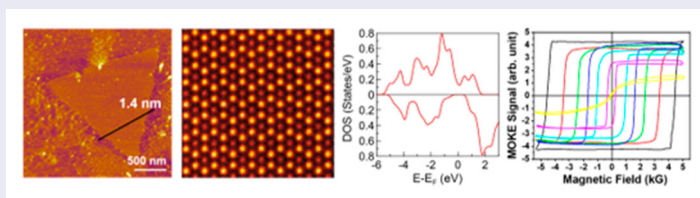
IMPACT STATEMENT
A T_C of 180 K, a perpendicular anisotropy of $7 \times 10^5\,J\,m^{-3}$, and a high coercivity of ~ 4.6 kG were achieved in covalent Cr_2Te_3 2D ferromagnets.

1. Introduction

The recent discovery of 2D vdW magnets such as CrI_3, $CrGeTe_3$, Fe_3GeTe_2, $MnPS_3$ and $FePS_3$ [1–3], has intensified research in 2D magnetism and spurred interests in searching for 2D magnets with novel properties. 2D magnets have potential technological impact not only because they represent the ultimate scaling limit in data storage and computing devices, but also due to their sensitivity to external perturbations such as electric gating [4,5].

They can further be integrated into vdW heterostructures, allowing the tuning of magnetic and topological order [6,7], valley splitting and polarization using proximity effects [8,9].

The vdW 2D magnets exfoliated from bulk crystals [10] suffer drawbacks such as poorly controlled layer thickness, size and shape in a single flake, low magnetic ordering temperature, and mostly antiferromagnetic interlayer coupling. To address such limitations,

---

it is desirable to explore material systems beyond vdW crystals. To this end, a class of covalent magnetic transition metal chalcogenides exemplified by Fe_xSe_y and Cr_xTe_y are worth exploring [11,12]. They possess a structure with monolayers of $FeSe_2$ and $CrTe_2$ intercalated by a layer of transition metals with ordered vacancies. The weakened interlayer bonding due to cation vacancies thus offers the possibility to obtain 2D magnets. Previously, we reported a giant coercivity of 4 Tesla and a transition temperature above 300 K in chemically synthesized Fe_3Se_4 nanostructures down to a few unit cell thickness [13]. Chemically synthesized Cr_2Te_3 nanostructures, thin films grown by molecular beam epitaxy, and 2D layers synthesized by chemical vapor deposition (CVD) have been reported recently [14–17]. However, systematic theoretical and experimental studies on the magnetic behavior of atomically-thin Cr_2Te_3 are so far lacking.

In this work, we report a concerted theoretical and experimental investigation of magnetism in 2D Cr_2Te_3 synthesized by CVD down to a single unit-cell thickness. Theoretical calculation predicts ferromagnetic order with an estimated T_C of ~ 200 K and a large perpendicular magnetocrystalline anisotropy of up to 1.1×10^6 J m^{-3} in the bulk, while making a surprising transition to in-plane anisotropy for atomically-thin Cr_2Te_3 from mono- to quad-layers. A collinear ferromagnetic spin arrangement is found for atomically-thin Cr_2Te_3, despite spin canting in the bulk. A half-metallic behavior, absent in bulk Cr_2Te_3, is predicted to emerge in atomically-thin layers and strengthened by reducing thicknesses. Experimentally, we found a T_C of ~ 180 K, a perpendicular anisotropy of 7×10^5 J m^{-3} and a coercivity of 4.6 kG at 20 K, from both ensemble magnetic measurements and magneto-optical Kerr effect (MOKE) measurements on single 2D crystals. Our work suggests that expanding beyond vdW materials is promising for discovering 2D magnets with unconventional properties.

2. Results and discussion

Atomically-thin Cr_2Te_3 crystals were prepared by CVD incorporating a space-confined strategy [18]. In this process, the precursors including Te and $CrCl_3$ powder mixed with NaCl were heated in separate temperature zones of a tube furnace. A schematic of the growth process is shown in Figure 1(a) and details of the growth are provided in the Supporting Information (SI). To obtain 2D layers of covalent Cr_2Te_3, the thermodynamic 3D growth needs to be suppressed and thus the growth should be kinetically controlled. The space-confined strategy deploys two substrates stacked together to introduce a local environment of precursor vapor in

between (Figure 1(b)) [18]. Comparing with the conventional technique (Figure 1(c)), this method can lead to more stable and slower gas flow, and thereby sustain a more steady and suppressed growth rate [19,20]. The decreased nucleation density is preferred for lateral growth as edge sites are more reactive. Meanwhile, new nucleation on top of 2D layers is discouraged due to weak inter-layer bonding and vapor concentration below the nucleation threshold. Moreover, the vdW mica substrate improves the mobility of the precursor atoms. The combined effects result in atomically-thin flakes as shown in the optical microscope image (Figure 1(d)). By comparison, using the conventional approach, the density of the crystals obtained is much higher and the thicknesses are also larger (Figure 1(e)). Figure 1(f,g) show a typical atomic force microscope (AFM) image and the corresponding height profile of a single Cr_2Te_3 flake. The thickness is found to be ~ 1.4 nm, which corresponds to a one-unit cell thick Cr_2Te_3 crystal consisting of a bilayer $CrTe_2$ and a Cr layer with vacancies in between (Figure 2(b)).

Atomically resolved high angle annular dark field scanning transmission electron microscopy (HAADF-STEM) measurements and energy dispersive X-ray spectroscopy (EDS) mapping were carried out to determine the crystal structure and elemental composition of the as-synthesized 2D crystals. Cr_2Te_3 possesses a hexagonal structure with a $\dot{P}$-31c (No. 163) space group ($a = 6.8$ Å, $c = 12.1$ Å). The Cr atoms classified by different Cr neighbors within the unit cell are labeled as Cr_I, Cr_{II} and Cr_{III} (see Figure 2(a,b)). Cr_I is located in between the $CrTe_2$ monolayers with ordered vacancies, whereas Cr_{II} and Cr_{III} are in the $CrTe_2$ layer. Cr_{II} has no Cr neighbor and Cr_{III} has only one Cr_I neighbor along the c axis. Cr_I atoms have two Cr_{III} neighbors along the c axis but no direct Cr neighbor in the ab plane. In the top view of the crystal structure (Figure 2(a)), the octahedral sites form a hexagon with two equilateral triangles connecting the three bottom and three top Te atoms, respectively. Therefore, as manifested in the HAADF-STEM image (Figure 2(c)) and corresponding atom-by-atom EDS mapping (Figure 2(d)), the Cr and Te columns can be clearly seen to form a hexagonal pattern with alternating dim (Cr columns) and bright spots (Te columns). This is in accordance with the (100) crystal planes of hexagonal structured Cr_2Te_3 (PDF#29-0458). The HAADF-STEM and atomic EDS mapping also synergistically indicate that there is no Te/Cr intermixing, consistent with our atomic Cr_2Te_3 model and excluding the existence of anti-site defects. Furthermore, the corresponding Fast Fourier Transform (FFT) pattern (the upper right inset of Figure 2(c)) reveals a single set of spots with an in-plane three-fold symmetry, which is in
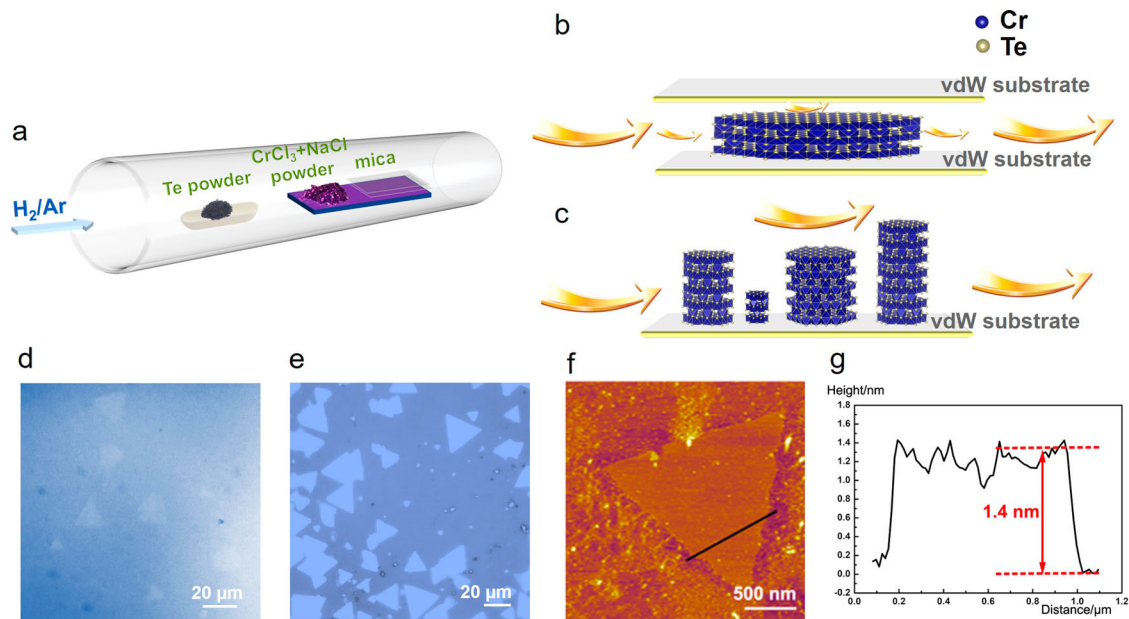
Figure 1. a, A schematic diagram of the CVD growth process. Schematic illustrations of the growth processes of Cr_2Te_3 using b, space-confined and c, conventional CVD, respectively. An optical microscope image of Cr_2Te_3 grown on mica utilizing d, the space-confined CVD and e, conventional CVD process. f, An AFM image and g, The height profile of a single Cr_2Te_3 flake. The thickness is $\sim$ 1.4 nm, corresponding to a single unit cell.
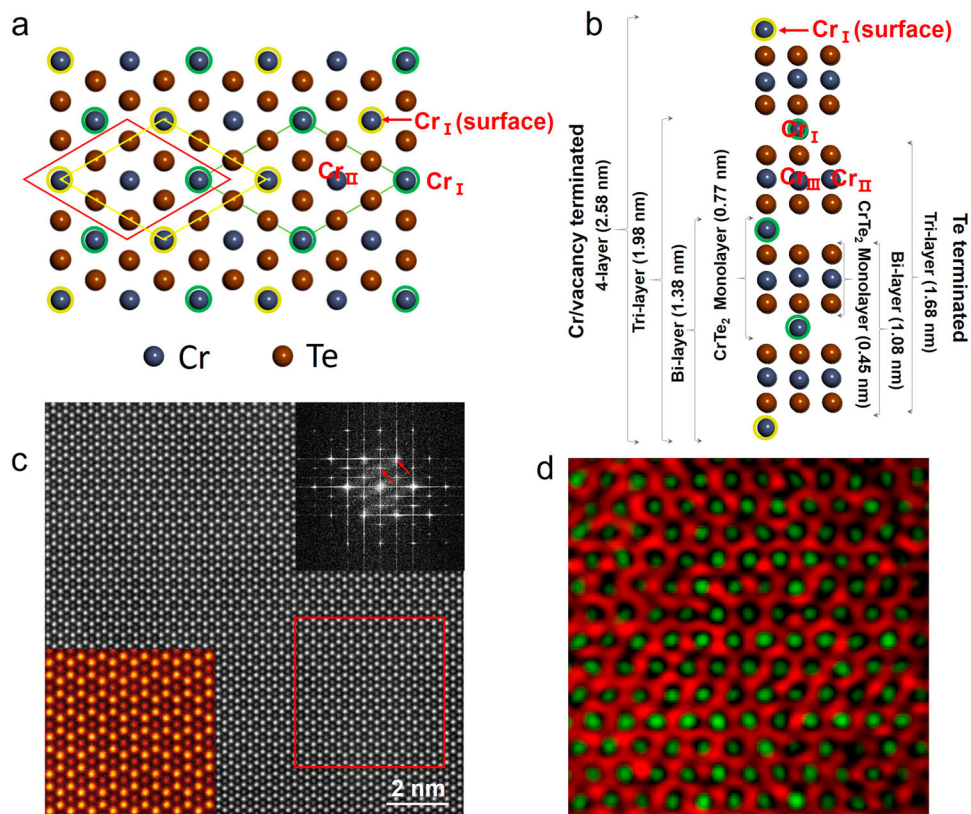

Figure 2. a, c-axis projection: unit cell of Cr_2Te_3 is shown in the red box; atoms with green halo are Cr_I atoms in the interior Cr/Vacancy layers; atoms with yellow halo are Cr_I atoms on the surface Cr/Vacancy layers. b, a-axis projection: braces show the structures used in calculations of single- to quad-layer. The Cr and Te columns are denoted by blue and brown solid columns, respectively. c, Atomically resolved HAADF-STEM image of single crystal Cr_2Te_3. Upper right inset: the reciprocal lattice obtained from an FFT of the HAADF-STEM image, with the lattice planes of Cr_2Te_3 highlighted by red arrows. Lower left inset: an enlarged image of c. d, EDS elemental mapping of the area shown by the red square in c. Green: Cr, Red: Te.

agreement with the (120) and (300) lattice periodicity of Cr_2Te_3. EDS mapping of Cr and Te of another triangular crystal is shown in Figure S1. The ratio of Cr and Te is determined as 0.67, consistent with the stoichiometry of Cr_2Te_3.

To model atomically-thin Cr_2Te_3, we consider thin films with mono-, bi-, tri- and quad- layers of $CrTe_2$ intercalated by a layer of Cr with ordered vacancies (a bi-layer corresponds to a single unit cell in bulk Cr_2Te_3). The top and bottom surfaces can be terminated by either Te or Cr atoms. The calculated thicknesses of 1–4 layers terminated by either Te or Cr/vacancy are shown in Figure 2(b). Layers terminated by Te atoms experience substantial in-plane contraction compared to bulk Cr_2Te_3, and are thus not stable in the 2D limit. However, if these 1–4 layers are terminated with partially filled Cr layers, the surface tension is substantially smaller, and the lattice parameters become closer to those of bulk Cr_2Te_3. Therefore, in subsequent calculations, these atomically-thin Cr_2Te_3 layers are modeled as being terminated by Cr with ordered vacancies.

From the DFT calculations, magnetic moments of 3.045, 3.126 and 3.096 μ_B are found for Cr_I, Cr_{II}, and Cr_{III} respectively in bulk Cr_2Te_3. The Te atoms are antiferromagnetically polarized with a moment of -0.195 μ_B. The total magnetization per unit cell (8 Cr and 12 Te atoms) is thus 24.23 μ_B, equivalent to 3.03 μ_B per Cr assuming a co-linear spin orientation. The calculated magnetization is substantially higher than the experimental value. This can be attributed to spin canting of the Cr atoms in between the $CrTe_2$ layers [21], as discussed later.

The exchange interactions were evaluated using total energy calculations for fully relaxed magnetic configuration at experimental lattice parameters. The pair exchange interactions were mapped onto the Heisenberg model with two nearest neighbors. The Heisenberg model total energy is

$$H = -\sum_{i>j}^{NN} J_{ij} \overrightarrow{S_i} \cdot \overrightarrow{S_j}, \qquad (1)$$

where J_{ij} are pair exchange parameters and $\overrightarrow{S_i}$ are unit vectors representing the direction of local magnetic moments. The calculated on-site exchange parameters $\left(J_0 = -\sum_j^{NN} J_{0j}\right)$ for different Cr sites of 1–4 layers together with that of bulk Cr_2Te_3 are given in Table S1. The magnetization and magnetic anisotropy energy (MAE) are shown in Table 1.

The Heisenberg model considering only the nearest neighbor and second nearest neighbor exchange interactions predicts a canted spin structure in bulk Cr_2Te_3,

Table 1. Magnetization and MAE of 1–4 layers together with bulk Cr_2Te_3.

	1-L (FM)	2-L (FM)	3-L (FM)	4-L (FM)	Bulk (canted)
M (μ_B unit cell^{-1})	18	30	42	54.15	19.2
M (10^3 A m^{-1})	538	500	488	483	365
MAE (meV unit cell^{-1})	-8.4	-9.6	-4.87	~ 0	3.5
MAE (MJ m^{-3})	-5.3	-4.1	-0.9	-2.6×10^{-5}	1.11

Notes: The unit cell is shown in the rhombic box in Figure 2(a). For 1–4 layers, the thickness of the unit cell is the thickness of the layers shown in Figure 2(b). For bulk Cr_2Te_3, the thickness of the unit cell corresponds to that of a bi-layer without the surface Cr atoms.
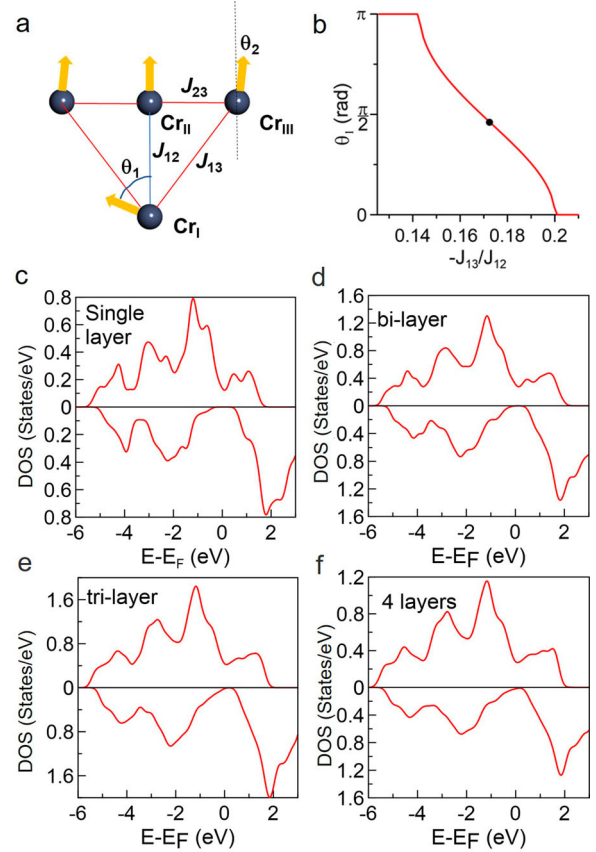

Figure 3. Competition of spin exchange, spin canting and spin-resolved total density of states (DOS). a, Schematic representation of exchange coupling in Cr_2Te_3. Competing inter-layer exchange parameters J_{12} and J_{13} induce canting angles θ_1 for Cr_I and θ_2 for Cr_{III} atoms. b, θ_1 as a function of the ratio of next-nearest to nearest neighbor exchange parameters J_{12}/J_{13}; the black dot represents θ_1 calculated from J_{12}/J_{13} obtained using the experimental lattice constant. Spin-resolved total DOS of c, single, d, bi-, e, tri-layer and f, quad-layers Cr_2Te_3 calculated for Cr-terminated structures. Majority DOS is shown in the upper panels while minority DOS is shown in the lower panels. E_F is the Fermi energy.

as shown schematically in Figure 3(a). It is found that $J_{12} = -3.25$ meV, $J_{13} = 1.25$ meV, $J_{23} = 2.92$ meV. The competing exchange interactions lead to spin frustration and canting, primarily for Cr_I atoms in the vacancy layer,
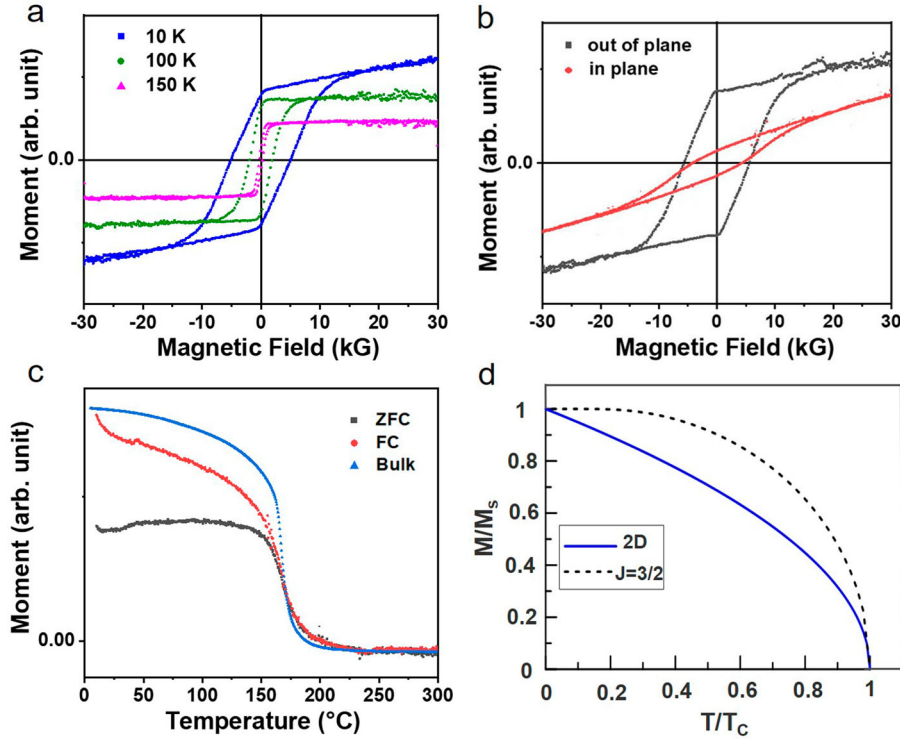
Figure 4. a, Out-of-plane magnetic hysteresis loops measured at different temperatures. b, Out-of-plane and in-plane magnetic hysteresis loops acquired at 10 K. c, ZFC and FC magnetization curves. The FC magnetization of a bulk film is also included for comparison. d, Calculated reduced magnetization as a function of reduced temperature of 2D (blue) compared to its 3D counterpart ($J = 3/2$, black) in the mean field approximation.

with much smaller angle for Cr_{III}. As can be seen from Figure 3(b), canting of Cr_I occurs at relatively large range of J_{13}/J_{12} values. At low J_{13}, coupling is antiferromagnetic, which switches to ferromagnetic as J_{13} increases. The black dot represents the canting angle $\theta_1 \sim 81°$ of Cr_I calculated from the exchange parameters obtained using the experimental lattice constant. This leads to a significant reduction of magnetization to 19.2 μ_B/unit cell (2.37 μ_B per Cr), or 365×10^3 A m^{-3} (Table 1).

Interestingly, spin canting is suppressed in mono- to quad-layers (i.e. collinear ferromagnetic). More strikingly, the 2D Cr_2Te_3 layers exhibit half-metallic behavior; *i.e.* they possess a metallic density of states (DOS) in one spin band and are insulating in the other [22], despite being metallic in bulk Cr_2Te_3. As shown in Table 1, the total magnetic moment per unit cell are 18, 30 and 42 μ_B for the mono-, bi- and tri-layer, respectively. An integer spin moment is a hallmark of half-metallic behavior [23].

As can be seen from the spin-resolved total DOS in Figure 3(c–e), a gap clearly exists in the minority DOS for mono-, bi- and tri- layer Cr_2Te_3, confirming their half-metallicity. In the quad-layer, the gap shrinks to near zero (Figure 3(f)). In bulk Cr_2Te_3, such a gap is absent (Figure S3b); however, the minority DOS is extremely low near the Fermi level, suggesting a high spin polarization.

Unlike in conventional materials where half-metallic behavior is weakened or destroyed at the surface or interface, the half-metallic behavior in 2D Cr_2Te_3 is strengthened by an increase of the gap with decreasing layer thickness [24]. This is due to the lower coordination number in atomically-thin layers, which narrows the band dispersion. The unique 2D half-metallicity in Cr_2Te_3 makes it promising as an electrode for magnetic tunnel junctions and spin transistors to realize 100% spin-polarized carrier transport [25].

MAE (Table 1) is strongly perpendicular for bulk Cr_2Te_3. Its magnitude is about 1×10^6 J m^{-3}, of the same order to those of permanent magnets [26]. The large MAE originates from the hexagonal structure and strong spin-orbit coupling due to the presence of heavy element Te. Strikingly the anisotropy turns in-plane (negative) for mono- to quad-layer Cr_2Te_3 as shown in Table 1, a behavior that is not understood at present. The MAE is negligibly small for the quad-layer, suggesting that it is close to the critical thickness to a transition from in-plane to perpendicular anisotropy.

The Curie temperature estimated from the on-site exchange parameter as $T_C = \frac{2J_0}{3k_B}$ is ~ 306 K for bulk Cr_2Te_3, which increases slightly in 2D layers. This is contrary to the behavior of most 2D magnets which
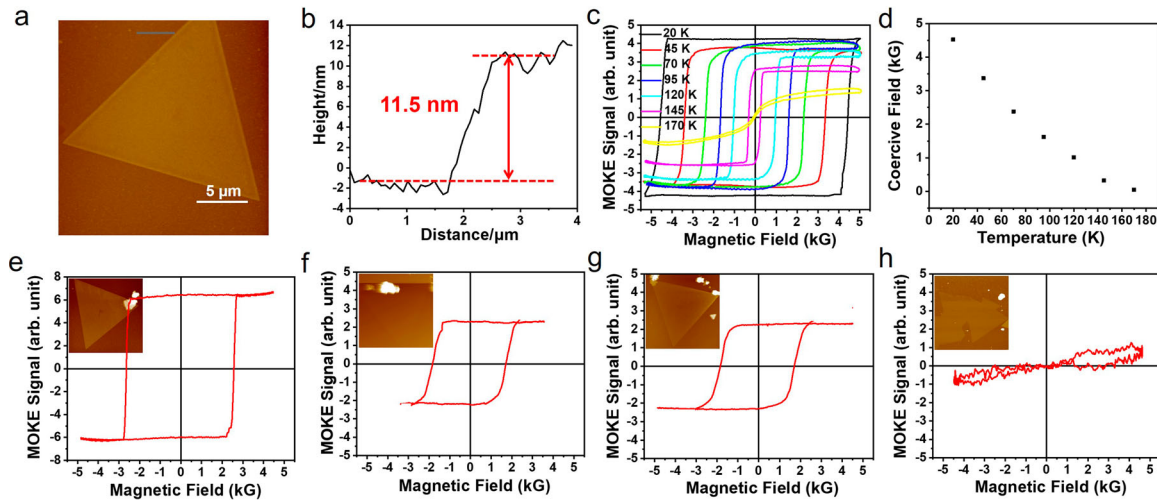
Figure 5. a, AFM image and b, the corresponding height profile of a single Cr_2Te_3 crystal, which shows a thickness of 11.5 nm. The black line in a corresponds to the height profile of b. c, normalized MOKE hysteresis loops and d, temperature-dependent coercivity of the corresponding Cr_2Te_3 crystal. e, f, g, h, MOKE hysteresis loops of Cr_2Te_3 2D crystals with different thicknesses, 25.2, 12.2, 7.8, and 2.8 nm, respectively. e–g were measured at 120 K; h was measured at 20 K. Inset: AFM images of the corresponding Cr_2Te_3 crystals.

show reduced T_C. Note that mean-field results typically overestimate T_C by 30–40%. Thus the experimental T_C is expected to be around 200 K for both 2D and bulk Cr_2Te_3.

The magnetic hysteresis loops of an ensemble of 2D Cr_2Te_3 crystals on mica were measured. Figure 4(a) shows the out-of-plane magnetic hysteresis loops for Cr_2Te_3 at temperatures from 10 to 150 K. A coercivity (H_C) of 4.6 kG at 10 K is observed, about 60% smaller than the 1.3 Tesla of bulk films (see Figure S6, SI). The smaller H_C can be explained by lower coordination numbers at sharp corners and edges of 2D crystals, which create local anisotropy smaller than that of the interior and lead to nucleation and propagation of magnetic domains at fields smaller than the anisotropy field. The 10 K loop shows a linear slope persisting to high fields, similar to that of thick films (Figure S6, SI). This slope is attributed to spin canting discussed in the theory section above. With a canting angle of 81°, contribution of the Cr_I moment to the total magnetization is insignificant at zero field. With increasing field, however, the spins of Cr_I atoms tilt slightly towards the z-axis, progressively increasing the magnetization. To estimate the value of MAE, both in-plane and out-of-plane hysteresis loops were measured at 10 K and displayed in Figure 4(b). Clearly the sample shows uniaxial anisotropy with an easy axis perpendicular to the plane, as evidenced by a perpendicular loop that is squarer and a parallel loop with smaller opening and lower remanent magnetization. By extrapolating both hysteresis loops to high fields, the anisotropy field is estimated to be 5.5T. Combining the saturation magnetization (M_S) of 240×10^3 A m^{-1} measured from a bulk film (see SI), the uniaxial MAE

is estimated to be 7×10^5 J m^{-3}. This is slightly smaller than the predicted value, but of the same order to that of hard magnetic CoPt and NdFeB [27]. The appreciable MAE plays a crucial role in stabilizing the long-range magnetic order in 2D Cr_2Te_3.

Figure 4(c) displays the field-cooled (FC) and zero-field-cooled (ZFC) magnetization as a function of temperature, which confirms the magnetic transition at around 180 K. Due to the small interlayer exchange, the magnetic ordering in the bulk is driven by exchange interactions in the $CrTe_2$ layer, and thus T_C barely changes from bulk to atomically-thin layers. Comparing the FC curves of 2D crystals with that of the bulk film, it can be seen that the magnetization drops faster at low temperatures but more gradually near T_C. This is confirmed by calculations based on mean-field approximation (Figure 4(d)) showing the transition near T_C to be more abrupt for the 3D than the 2D case, mimicking experimental results. At temperatures below 30 K, a sharp rise in magnetization is observed in the FC curve. This is attributed to edge spins with weaker exchange coupling than the interior, leading to disorder [28]. The behavior of the ZFC curve, on the other hand, is quite different from that of conventional ferromagnets. It shows a plateau in a broad temperature range, and decreases slightly with further decreasing temperature. This can be understood as the competition between increasing spin canting and decreasing spin disorder with decreasing temperature.

Polar magneto-optical Kerr effect (MOKE) microscopy was used to extract magnetic properties of individual 2D crystals. The same 2D crystals were then imaged by AFM to correlate their hysteresis behaviors

with their morphologies. The MOKE hysteresis at different temperatures on a 2D crystal with a thickness of 11.5 nm shown in Figure 5(a) are plotted in Figure 5(c). The behavior is consistent with ensemble measurements with similar H_C values. At low temperatures, the single crystal shows a square loop, with near unity remanence ratio M_r (remanent/saturation magnetization) and a sharp transition near H_C, resulting from the perpendicular anisotropy. With increasing temperature, the loops become more rounded, with decreasing M_r and H_C. At 170 K, the flake becomes nearly paramagnetic with negligible H_C. Temperature dependent H_C plotted in Figure 5(d) shows a rapid drop of H_C with increasing temperature. In a material with uniaxial anisotropy, MAE scales with M_S^3, which explains the sensitive temperature dependence of H_C [27].

Hysteresis loops of representative 2D crystals with different thicknesses were further measured, as shown in Figure 5(e–h). As the thickness of the flakes decreases from 25.2 to 7.8 nm, the square hysteresis behavior measured at 120 K changes only slightly, owing to the robust perpendicular anisotropy. A small drop in H_C is observed with decreasing thickness. However, a change of behavior is observed for the 2.8 nm crystal (two unit cell thickness). The MOKE signal becomes so weak at 120 K that no clear hysteresis can be detected. At 20 K, while the low signal-to-noise ratio prevents the exact shape of the hysteresis to be resolved, it clearly deviates from the square loops observed for thicker crystals with negligible M_r and H_C. This seems to be consistent with the theoretical prediction of a transition from the perpendicular to in-plane anisotropy in the quad-layer Cr_2Te_3.

3. Conclusion and outlook

In conclusion, 2D ferromagnetic Cr_2Te_3 crystals were realized by controlling the kinetic growth in a CVD process. The resulting 2D crystals demonstrate large magnetic anisotropy, which helps to stabilize the ferromagnetic order in 2D Cr_2Te_3. First-principles calculations further predict an unconventional half-metallicity, existing only in 2D layers and strengthened by reduced dimensions. Our work represents an important step towards the applications of 2D Cr_2Te_3 and related compounds for spintronics, and will inspire the search for new covalent 2D magnets.

Disclosure statement

No potential conflict of interest was reported by the author(s).

References

[1] Wang M-C, Huang C-C, Cheung C-H, et al. Prospects and opportunities of 2D van der Waals magnetic systems. Ann Phys (Berlin). 2020;532(5):1900452.

[2] Mak KF, Shan J, Ralph DC. Probing and controlling magnetic states in 2D layered magnetic materials. Nat Rev Phys. 2019;1(11):646–661.

[3] Gibertini M, Koperski M, Morpurgo AF, et al. Magnetic 2D materials and heterostructures. Nat Nanotechnol. 2019;14(5):408–419.

[4] Deng Y, Yu Y, Song Y, et al. Gate-tunable room-temperature ferromagnetism in two-dimensional Fe_3GeTe_2. Nature. 2018;563(7729):94–99.

[5] Huang B, Clark G, Klein DR, et al. Electrical control of 2D magnetism in bilayer CrI_3. Nat Nanotechnol. 2018;13(7):544–548.

[6] Zhang W, Zhang L, Wong PKJ, et al. Magnetic transition in monolayer VSe_2 via interface hybridization. ACS Nano. 2019;13(8):8997–9004.

[7] Zhang R-X, Cole WS, Wu X, et al. Higher-order topology and nodal topological superconductivity in Fe(Se,Te) heterostructures. Phys Rev Lett. 2019;123(16):167001.

[8] Norden T, Zhao C, Zhang P, et al. Giant valley splitting in monolayer WS_2 by magnetic proximity effect. Nat Commun. 2019;10(1):4163.

[9] Zhao C, Norden T, Zhang P, et al. Enhanced valley splitting in monolayer WSe_2 due to magnetic exchange field. Nat Nanotechnol. 2017;12(8):757–762.

[10] Cortie DL, Causer GL, Rule KC, et al. Two-dimensional magnets: forgotten history and recent progress towards spintronic applications. Adv Funct Mater. 2020;30(18): 1901414.

[11] Kawaminami M, Okazaki A. Neutron diffraction study of Fe_7Se_8. II. J Phys Soc Jpn. 1970;29(3):649–655.

[12] Andersen AF. The magnetic structure of Cr_2Te_3, Cr_3Te_4, and Cr_5Te_6. Acta Chem Scand. 1970;24(10):3495–3509.

[13] Zhang H, Long G, Li D, et al. Fe_3Se_4 nanostructures with giant coercivity synthesized by solution chemistry. Chem Mater. 2011;23(16):3769–3774.

[14] Wang F, Du J, Sun F, et al. Ferromagnetic Cr_2Te_3 nanorods with ultrahigh coercivity. Nanoscale. 2018;10(23): 11028–11033.

[15] Roy A, Guchhait S, Dey R, et al. Perpendicular magnetic anisotropy and spin glass-like behavior in molecular beam epitaxy grown chromium telluride thin films. ACS Nano. 2015;9(4):3772–3779.

[16] Wen Y, Liu Z, Zhang Y, et al. Tunable room-temperature ferromagnetism in two-dimensional Cr_2Te_3. Nano Lett. 2020;20(5):3130–3139.

[17] Ramasamy K, Mazumdar D, Bennett RD, et al. A. Syntheses and magnetic properties of Cr_2Te_3 and $CuCr_2Te_4$ nanocrystals. Chem Commun. 2012;48(45):5656–5658.

[18] Zhou S, Wang R, Han J, et al. Ultrathin non-van der Waals magnetic rhombohedral Cr_2S_3: space-confined chemical vapor deposition synthesis and Raman scattering investigation. Adv Funct Mater. 2019;29(3):1805880.

[19] Zhang Y, Yao Y, Sendeku MG, et al. Recent progress in CVD growth of 2D transition metal dichalcogenides and related heterostructures. Adv Mater. 2019;31(41): 1901694.

[20] Zhou S, Gan L, Wang D, et al. Space-confined vapor deposition synthesis of two dimensional materials. Nano Res. 2018;11(6):2909–2931.

[21] Hamasaki T, Hashimoto T, Yamaguchi Y, et al. Neutron diffraction study of Cr_2Te_3 single crystal. Solid State Commun. 1975;16(7):895–897.

[22] Katsnelson MI, Irkhin VY, Chioncel L, et al. Half-metallic ferromagnets: from band structure to many-body effects. Rev Mod Phys. 2008;80(2):315–378.

[23] Pickett WE, Moodera JS. Half metallic magnets. Phys Today. 2001;54(5):39–45.

[24] Brener NE, Tyler JM, Callaway J, et al. Electronic structure and Fermi surface of CrO_2. Phys Rev B. 2000;61(24):16582–16588.

[25] Bratkovsky AM. Tunneling of electrons in conventional and half-metallic systems: towards very large magnetoresistance. Phys Rev B. 1997;56(5):2344–2347.

[26] Weller D, Moser A, Folks L, et al. High K_u materials approach to 100 Gbits/in^2. IEEE T Magn. 2000;36(1): 10–15.

[27] Mryasov ON, Nowak U, Guslienko KY, et al. Temperature-dependent magnetic properties of FePt: effective spin Hamiltonian model. Europhys Lett. 2005;69(5):805–811.

[28] Westman C, Jang S, Kim C, et al. Surface induced suppression of magnetization in nanoparticles. J Phys D: Appl Phys. 2008;41(22):225003.